Journal of Offshore Mechanics and Arctic Engineering. Received March 29, 2019;
Accepted manuscript posted November 19, 2019. doi:10.1115/1.4045625

Investigation of nonlinear wave-ice interaction using parameter study and numerical simulation

Moritz C. N. Hartmann *
Ship Structural Design and Analysis
Hamburg University of Technology
Hamburg, Germany
Email: m.hartmann@tuhh.de

Franz von Bock und Polach
Ship Structural Design and Analysis
Hamburg University of Technology
Hamburg, Germany
Email: franz.vonbock@tuhh.de

Sören Ehlers
Ship Structural Design and Analysis
Hamburg University of Technology
Hamburg, Germany
Email: ehlers@tuhh.de

Norbert Hoffmann
Structural Dynamics
Hamburg University of Technology
Hamburg, Germany
Email: norbert.hoffmann@tuhh.de

Miguel Onorato
Dipartimento di Fisica Generale
Università di Torino
Torino, Italy
Email: miguel.onorato@unito.it

Marco Klein
Ship Structural Design and Analysis
Hamburg University of Technology
Hamburg, Germany
Email: marco.klein@tuhh.de

This paper investigates the question of the existence of nonlinear wave-ice interaction with the focus on nonlinear wave propagation and dispersion of waves. The scope of this investigation is to provide a better understanding of ice and wave conditions required to observe nonlinear wave effects under level ice.
Direct numerical simulations of nonlinear waves in solid ice are performed within the weakly Nonlinear Schrödinger Equation framework, by using the theoretical findings from Liu and Mollo-Christensen's 1988 paper.
Systematic variations of wave and ice parameters address the impact of the mechanical ice properties and ice thickness on traveling waves of certain wave lengths. The impacts of parameters characteristics on nonlinear focusing and wave dynamics, as well as possible constraints regarding physical consistency, are discussed. It is presented that nonlinear focusing in level ice occurs theoretically. Hereby, distinctive areas of validity with respect to nonlinear wave focusing are identified within the parameter study, which strongly depends on the material properties of the level ice.
The results obtained in the parameter study are subsequently used to investigate wave focusing under level ice. Therefore, an exact solution of the NLSE, the Peregrine breather, is utilized. The analytical solution for level ice is compared to the open water solution and accompanied by direct numerical simulations. These investigations show that nonlinear wave focusing can be predicted under level ice for certain parameters. In addition, the agreement of the direct simulations and the analytic solution verifies the numerical approach for nonlinear waves in solid ice.

Introduction

The climate in cold regions is subjected to changes where waves and ice increasingly interact. Extratropical storm tracks are an important driver for the weather and wave conditions in the Northern hemisphere. The change of these

*Address all correspondence to this author.

tracks, caused by a poleward shift and intensification of the North Pacific cyclones and a southern extension of the North Atlantic storm tracks, is represented in recent climate models, see e.g. Harvey [1].

Furthermore, the climate changes towards a state with increasing global sea surface temperature, which is well known and exposed for example in the US Climate science special report [2] and the Intergovernmental Panel on Climate Change report [3]. This directly affects the seasonal sea ice distribution in the arctic and antarctic regions. The seasonal variability of sea ice concentration and the changes of wave field impacting drivers promotes the increase of the wave-ice interaction.

Li et al. [4] use buoy and altimeter data, as well as numerical simulations to investigate the wave climate in the Arctic sea. The results indicate that the significant wave height and the retreating ice coverage are positively correlated. This is mostly due to the extended fetch area which is available due to the decreased Arctic ice sheet. If the ice area decrease further in the future, the authors project a more frequent occurrence of large waves by an increase of the growth rate of the significant wave height.

However, the trend and governing parameters of wave-ice interaction are not yet uniquely defined. Contrary to the previous studies, the research of Morim et al [5] shows a robust projected decrease of the significant wave height in the North Atlantic region in the seasonal analysis. The coherent, using a multi-method ensemble of global climate projections and community driven study applies a high emission scenario. From the results it can be concluded that climate model driven uncertainties cause mainly the differences in current wind-wave climate projections.

Stephenson, et al. [6] predict significant increase of maritime transportation with low ice class ships along all relevant Arctic sea routes, namely the Northern sea route, the Northwest passage, the Arctic Bridge and the North Pole route. Especially in the US, Russia, Greeceland and Canada, the access to the countries exclusive economic zones via low ice class ships raise in a range of 5% to about 30%. The sea trade and its capability on the Northern sea route is reviewed in detail by Liu and Kronbak [7].

Consequently, the knowledge in the field of naval architecture and ocean engineering in terms of ship design and construction, structural analysis and hydrodynamics for ships and marine structures in ice environment has to increase significantly. New methods for the quantification of the quality of arctic ship design are provided by von Bock und Pollach et al. [8]: to compare different ship designs, the authors introduce the ship merit factor in ice.

For the approximation of wave propagation in well defined parameter regimes, the superposition of linear waves can be used. A physical consistent, high-order accuracy model, however, needs to take high-order terms into account. By the mathematical occurrence of nonlinear terms, the physical occurrence of interactions between the superposed linear wave contributions is represented which allows to take e.g. steep waves and breaking events into account [9, 10].

Until now, the process of nonlinear wave propagation in an ice covered environment is not completely understood. Theoretical investigations of nonlinear wave events in ice was done by several researchers. For example Liu and Mollo-Christensen [11] studied nonlinear wave effects theoretically on the basis of the RV Polarsten report. Further investigations, whether nonlinear effects occur with respect to waves in ice, were done by Collins et al. [12] and Kohout et al. [13]. Whereas Collins et al. analysis is based on the report of RV Lance, Kohout et al. used the report of the icebreaker Aurora Australis. But neither the way of propagation, nor the change in distribution of the wave energy nor the incidence of nonlinear wave events has been completely clarified.

This paper connects both research fields by giving in section 2 and 3 a review in wave theories and ice material theories, presenting a numerical technique to investigate wave-ice interaction and discussing results of a parameter study in section 4. The conclusions are given in section 5.

Wave Theory

The Euler equation, describing fluid motion by pressure and volumetric forces in the absence of shear stress (inviscid fluid flow), is the starting point for wave theory. Under the claim of irrotational flow,

$$\nabla \times \mathbf{u} = 0, \tag{1}$$

the velocity vector field $\mathbf{u} = (u(x,z,t), w(x,z,t))^T$ is conservative and represents a potential field [14, 15]. Assuming that the velocity components are continuous and the domain is simply connected, Schwarz's theorem can be applied and the scalar velocity potential $\phi(x,z,t)$ is given by

$$\nabla\phi = \mathbf{u}. \tag{2}$$

Substituting the velocity potential in the solenoidal flow assumption results in the Laplace equation

$$\nabla \cdot \nabla\phi = \Delta\phi = 0 \tag{3}$$

which is generally used to describe wave motion, e.g. Whitham [16] and Kundu [17]. For surface gravity waves a phase-discontinuity, the free surface, is present and boundary conditions have to be formulated.

For potential flows the nonlinear boundary conditions in the sense of dynamic and kinematic constraints can be defined by using the surface's elevation $\zeta = \zeta(x,t)$ and the velocity potential.

The dynamic boundary condition is formulated in terms of Bernoulli's equation which can be derived from integrating the Euler equation assuming incompressible and irrotational flow and balancing along a streamline at the free surface.

The kinematic boundary condition originates from the Eulerian specification on the surface elevation.

At the free surface the nonlinear dynamic and kinematic boundary conditions yield

$$\frac{\partial \phi}{\partial t} + \frac{1}{2}\left(\nabla \phi\right)^2 + g\zeta = 0 \tag{4}$$

$$\frac{\partial \zeta}{\partial t} + \frac{\partial \phi}{\partial x}\frac{\partial \zeta}{\partial x} = \frac{\partial \phi}{\partial z}\,. \tag{5}$$

Furthermore, a boundary conditions at the bottom ($z = H$) have to be defined in terms of a Neumann condition for the velocity potential. Assuming a horizontal, impermeable bottom profile, the condition is necessarily and sufficiently defined by

$$\frac{\partial \phi}{\partial z}|_{z=H} = 0\,. \tag{6}$$

The Laplace equation can be solved by using the method of separation of variables and applying the combined surface boundary conditions, Eqs. (4) and (5), and bottom boundary condition, Eq. (6). The elevation at the surface ζ results from the free-surface condition. The velocity vector is derived from Eq. (2).

Starting with regular, sinusoidal waves the main characteristics are the wave length (or wave number), the frequency (or period) and the amplitude. Adding waves of different frequency and amplitude, one is able to reconstruct irregular waves. The principle of superposition is fundamental for the linear wave theory. With the use of Fourier transformation, complex sea states in time domain can be divided into their linear components in frequency domain. The inverse Fourier transformation converts the solutions in frequency domain back into time domain [18]. One important advantage of the frequency space is the representation of the wave by amplitude and phase in terms of Euler's formula and the resulting very efficient calculation of derivatives [15].

Nonlinear theory

With nonlinear theory more complex wave processes can be described. For steep, surface gravity waves, it is necessary to take the interactions between the superposed linear wave components into account. This can be done by applying a weakly nonlinear approach. In this context, *weak* implies the physical reduction of wave dynamic's nonlinearity. The first research on nonlinear wave theory was done in the 19th century, e.g. by Gerstner [19] and Stokes [20]. For deep water, weak nonlinearity and a narrow banded frequency range, the NLSE [21] appears, for shallow water, the Korteweg-deVries and Kadometsev-Petviashvili equations are found. In the present paper we want to focus on the one dimensional nonlinear Schrödinger equation in space domain (NLSE).

Space NLSE

By applying the method of multiple scales to the Euler equations, the nonlinear wave equations are derived, see Davey and Stewartson [22] and Holmes [23]. The time and space scales of the variables in the differential equations are expanded by slowly varying and independent time and space variables. By this, a scale separation is introduced which increases the degree of freedom in the differential equation system. The additional unknown variables of different scales can be closed by asymptotic approximations.

Thus, the expansion of the complex envelope $A(x,t)$ is used to approximate the surface elevation on infinite water depth

$$\zeta = \Big(|A| - \frac{1}{8}k_0^2|A|^3\Big)cos(\theta) + \frac{1}{2}k_0|A|^2 cos(2\theta) + \\ + \frac{3}{8}k_0^2|A|^3 cos(3\theta) + \text{h.o.t} \tag{7}$$

with the carrier wave number k_0, see Onorato et al. [24]. Equation (7) represents an approximation to the third order Stokes waves on deep water, if the complex envelope $A(x,t)$ is constant in time and space.

The angle θ is defined with the nonlinear dispersion relation Ω and the arbitrary wave phase φ as

$$\theta = k_0 x - \Omega t + \varphi\,,\ \Omega = \omega_0\Big(1 + \frac{k_0^2|A|^2}{2}\Big)\,. \tag{8}$$

The phase φ is a function of t and x and related to the complex envelope as

$$\varphi(x,t) = \arctan(\Im[A(x,t]/\Re[A(x,t)]. \tag{9}$$

The advantage of the additional scales is the ability to remove secular (nonperiodic) terms in the expansion series. This is done by the definiton of wave's amplitude and phase. In Eq. (7) it's shown that different wave modes occur, the phases and amplitudes of the higher, bounded harmonics depend on the primary, free wave mode (terms related to $cos(\theta)$).

For infinite water depth, the multiple scale method results in the NLSE, see Zakharov [21]. In 1D+t dimension, see Onorato et al. [24] and Osborne [10], the equation is given by

$$i\Big(\frac{\partial A}{\partial t} + c_g\frac{\partial A}{\partial x}\Big) - \alpha\frac{\partial^2 A}{\partial x^2} - \beta|A|^2 A = 0 \tag{10}$$

with

$$\alpha = \frac{\omega_0}{8k_0^2} \text{ and } \beta = \frac{\omega_0 k_0^2}{2} \tag{11}$$

The nondimensional form of the NLSE in moving frame of reference, see [24], is given by

$$i\frac{\partial A^*}{\partial t^*} - \frac{\partial^2 A^*}{\partial x^{*2}} - \text{BFI}^2|A^*|^2 A^* = 0 \tag{12}$$

with the nondimesional time, envelope and space variables marked with asterisk. The Benjamin-Feir index is given by

$$\mathrm{BFI} = 2k_0a_0(\Delta k/k_0)^{-1}\,, \tag{13}$$

assuming a characteristic length scale $L \sim \Delta k_{NLSE}^{-1}$, where Δk_{NLSE} is the typical bandwith for the wave length spectrum of surface gravity waves. The Benjamin-Feir index, respectively the ratio of nonlinearity and dispersion is an important parameter for the quantification of nonlinearity and instability of the NLSE, see Serio et al. [25].
In this study, the NLSE is solved by applying the pseudospectral split step Fourier method [26, 27], separating the calculation of linear and nonlinear part. While the nonlinear part is solved in time domain, the solution of the linear part is calculated in frequency domain after applying a Fourier transformation. The main advantages compared to standard finite difference schemes is its easy implementation and its computational efficiency.

Intense wave events

As a consequence of nonlinear wave interaction extreme wave events may occur. One of the main process driving these events is the modulational instability. Under the condition of anomalous dispersion, the perturbations of the wave envelope induces the amplifications in the amplitude and height of the wave signal [28]. In Benjamin and Feir [29] the instability of an open water, progressive wave of finite amplitude, the Stokes wave, is analyzed in terms of a basic wave train and a disturbing progressive wave pair which is characterized by small perturbations in wave number and side band frequencies. For arbitrary water depth the limit is found to be $k_0H > 1.363$, whereas for $k_0H < 1.363$ the waves are stable.
In the unstable case, the focusing regime is reached, whereas the stable case is characterized by reaching the defocusing regime, see Whitham [9].
The instability of the wave is also covered by the ratio of the coefficients characterizing the nonlinear and the dispersive term ($\sqrt{|\beta|/\alpha}$) (from now on 'focusing ratio'), see e.g. [25] for a discussion on arbitray water depth.
The limitation of focusing and defocusing regimes of deep water waves in ice are represented by limiting curves instead of a constant k_0H value. These curves represent where the focusing ratio equals zero and gives the functional dependence of ice thickness and wave number with respect to the investigated ice material properties. Thus, the discussion on the instability of open water waves in finite depth can be extended in this study to the instability of deep water waves in ice. Whereas the open water waves are limited by the water depth, the instability of the deep water waves in ice are limited by ice material and wave characteristics.
In the case of surface gravity waves the main consequence of weakly nonlinear interaction is the change in the wave speed (anomalous dispersion) regarding to the linear theory [30].

Nonlinear waves in ice

In the study of Liu and Mollo-Christensen [11] the propagation of waves in ice covered water was analyzed which has been mainly motivated by observations of the RV Polarstern. The observations indicated that ice on the water surface substantially affects the dynamics of the water waves. Under the assumption of potential flow and linearization, the dynamic boundary condition at the ice-bounded surface changes to

$$-\rho_w(\frac{\partial\phi}{\partial t} + g\zeta) = P_{ice}(d) = (\Gamma_B + \Gamma_C + \Gamma_I)\zeta. \tag{14}$$

The ice material properties and corresponding spatial and temporal derivatives are represented by Γ. The individual contributions of **B**ending, **C**ompression and **I**nertia are represented by

$$\Gamma_B = \delta\frac{\partial^4}{\partial x^4} \quad \Gamma_C = \gamma\frac{\partial^2}{\partial x^2} \quad \Gamma_I = \iota\frac{\partial^2}{\partial t^2}, \tag{15}$$

with the flexural rigidity δ, the compressive rigidity γ and the length scale of submerged ice portion ι

$$\delta = Ed^3(12(1-\nu^2))^{-1}\,, \quad \gamma = Pd\,, \quad \iota = \rho_i d. \tag{16}$$

Under normalization with the water density, the ice material properties **B**ending, **C**ompression and **I**nertia

$$B = \delta\rho_w^{-1}\,, \quad C = \gamma\rho_w^{-1}\,, \quad I = \iota\rho_w^{-1}\,, \tag{17}$$

can be derived, see Liu and Mollo-Christensen [11].
The Young's modulus of ice E, the thickness of the ice plate d, the compressive stress P, the dynamic Poisson's ratio for ice ν, the density of water ρ_w and ice ρ_i are discussed in Sec. 'Sea Ice'. By accounting for these properties, the dispersion relation yields

$$\omega_0 = (gk_0 + Bk_0^5 - Ck_0^3)^{\frac{1}{2}}(1+k_0I)^{-\frac{1}{2}}\,. \tag{18}$$

In Liu and Mollo-Christensen [11] the NLSE coefficients for ice covered surface are given by

$$\begin{aligned}\alpha = \quad & \frac{1}{8\omega_0^3(1+Ik_0)^4}\big(g^2(1+4Ik_0) \\ & -6gBk_0^4(5+8Ik_0+4(Ik_0)^2) \\ & +2gCk_0^2(3+2Ik_0+2(Ik_0)^2) - 3(Ck_0^2)^2 \\ & -(Bk_0^4)^2(15-20Ik_0+8Ik_0^2)\big)\end{aligned} \tag{19}$$

$$\begin{aligned}\beta = \quad & \frac{k_0}{\zeta_1^2 2g_0}(\zeta_1^2k_0^2c_{p,0} \\ & \cdot\big(g+127Bk_0^4-10C_0k_0^2-3Ck_0^2\big) \\ & -36k_0\zeta_2c_{p,0}(10Bk_0^4-C_0k_0^2) \\ & -2k_0\phi_2(7g+187Bk_0^4-25C_0k_0^2)\big)\end{aligned} \tag{20}$$

with the first and second-order amplitude approximations of the surface elevation ζ_1, ζ_2, the velocity potential $\phi_2$and the phase velocity $c_{p,0} = (g_0/k_0)^{1/2}$, with $g_0 = g + Bk_0^4 - C_0k_0^2$ and $C_0 = C + Ic_{p,0}^2$. The order-specific amplitudes result from expanding the quantities ϕ, ζ and c_p, substituting into the nonlinear, ice-cover affected, surface boundary conditions and the Laplace equation and solving according to the power of nonlinearity [11].

Sea Ice Properties and Conditions

Ice is a non-homogeneous and anisotropic material, however, due to the complexity of its properties and a lack of knowledge in certain areas, its properties are often simplified for engineering matters [31]. Moreover, a description of the complexity in depth may also not be necessary for many matters.

Here, the ice properties are referred to with their relevance for wave-ice interaction. Starting with the density, that can vary over a wide range with an approximated average value being $\rho_i = 910\,\mathrm{kgm}^{-3}$ [31]. Further relevant parameters are the elastic modulus, E, the brine volume ν_b and the Poisson's ratio ν. As summarized in Timco and Weeks [31] many properties are expressed by a semi-empirical function of the brine volume, which is the entrapped unfrozen saline liquid within the ice. The latter reduces the effective bulk material in the cross-section and therewith the nominal strength parameters. The brine volume is a function of the sea water salinity S_w, and the sea ice temperature T_i, which is between $-0.5\,^\circ\mathrm{C}$ and $-22.9\,^\circ\mathrm{C}$ [31]. Therefore, the brine volume depends on the geographic region of interest and is defined according to Frankenstein and Garner [32]

$$\nu_b = S_w \frac{49.185}{|T_i|} + 0.532. \tag{21}$$

The elastic modulus in GPa can be defined according to

$$E = 10 - 0.0351\nu_b \tag{22}$$

According to illustrations in Timco and Weeks [31] and Eq. (22) a value of 9 GPa is considered as an appropriate estimate for first year ice.

With respect to the stiffness of an ice plate and its bearing capacity (plate modulus) also the Poisson's ratio is a parameter of significance. In wave related problems addressed in this paper creep related effects are not accounted for and therewith the dynamic value of $\nu = 0.33$ is used [31].

Traditionally, in addition to elastic modulus and thickness, also the flexural strength is taken as a characteristic to classify an ice sheet's property. The flexural strength σ_f can be expressed as a function of the brine volume [33]

$$\sigma_f = 1.76^{-5.88\sqrt{\nu_b}}. \tag{23}$$

With respect to ship resistance, values from 500 kPa [34] to 600 kPa are typically used for first year winter ice.

Sea ice is subjected to wind forces that either introduce movements or generate compressive stresses in the ice. Those can reach values of the compressive strength of $P = 0.5\,\mathrm{MPa}$ to $P = 5\,\mathrm{MPa}$ [31], if the ice would not buckle before and create a ridged ice field.

For this study we make use of the values, which are provided by Liu and Molle-Christensen [11] and coherent to above defined parameter ranges: the ice density $\rho_i = 922.5\,\mathrm{kgm}^{-3}$, the Young's modulus $E = 6\,\mathrm{GPa}$, the Poisson ratio $\nu = 0.33$ and the compressive strength $P = 5.1\,\mathrm{MPa}$.As shown the parameters are coherent to previously defined parameter ranges.

Results and Discussion

In this section, first the ice thickness and wave number range, limited by rules of physical consistency, are identified in a parameter study. Secondly, representative results of the comparison between the Peregrine breather solution using NLSE with either open water, see Eq. (11), or ice boundary condition, see Eq. (19), are presented.

Parameter study

Weakly nonlinear, narrow banded waves can be sufficiently described by the NLSE. The occurrence of nonlinear wave events and their generation principle depends strongly on the wave group properties, namely carrier wave number k_0, group velocity c_g and carrier angular frequency ω_0. These are represented by the Benjamin-Feir index, Eq. (13), where the first contribution on the right hand side depends on the wave spectrum's bandwidth. The focusing parameter (β/α) gives the ratio of nonlinear and linear coefficients. This ratio represents the dependency of wave speed on amplitude and the changes in wave's dispersion. If this ratio is negative the wave groups are stable and the solutions are in the defocusing regime with occurrence of dark solitons and vortex structures [35]. A positive ratio implies instability, the solutions are of focusing type. Here, the nonlinear interactions between the wave modes cause a concentration of local energy and the unstable wave groups can form to extreme waves [24].

If the water surface is covered by solid ice, the wave dynamics differ from open water conditions. In the study of Liu and Mollo-Christensen [11], the flexural and the compressive strength and the length scale of submerged ice portion, referred to bending, compression and inertia, are taken into account for wave propagation.

In the following, the influence of the angular frequency, the ratio of group and phase velocity and the focusing ratio by varying wave number and ice thickness are analysed. Nonlinear focusing waves are localized by the occurrence of positive focusing ratio and physical consistent wave dispersion and propagation parameters. Furthermore, the role of material's contributions regarding the nonlinear wave dynamics in ice covered water can be analyzed.

In Tab. (1) the investigated cases in terms of accounted ice properties are summarized. The first block refers to

Table 1. Variation of assumed ice properties, **B**ending, **C**ompression and **I**nertia and corresponding figures. For '1' the appropriate term is taken into account, for '0' the term is set to zero.

case	B	I	C	Figures
I	1	0	0	(1.a), (3.a)
II	0	1	0	(1.c), (3.b)
III	1	1	0	(1.e), (3.c)
IV	0	0	1	(2.a), (4.a)
V	1	1	1	(2.b), (4.b)

the case of sole bending, sole inertia and the combination of both contributions. Properties regarding bending and inertia are of interest when investigating strength and failure mechanisms of an ice plate. In addition to this, the impact of compression due to ice ridge dynamics was analyzed [11]. Case IV represents the case where only compression affects the wave dynamics. The last case merges all properties and represents the reference case originally introduced by Liu and Mollo-Christensen [11].

Angular frequency and velocity ratio

In Figs. (1) and (2) the angular frequency (Subfigs. (1.a, c) and Subfigs. (2.a, c, e)) and the group to phase velocity ratio (Subfigs. (1.b, d) and Subfigs. (2.b, d, f)) are shown for the cases I to II and for the cases III to V, see Tab. 1.
For physical consistency the focus in the plots is put on small positive values of angular frequency and velocity ratio satisfying

$$\begin{aligned} \omega_0 &> 0 \\ \frac{c_g}{c_p} &> 0\,. \end{aligned} \tag{24}$$

The main idea of the following figures is to visualize the validity range for simulations of ice covered nonlinear waves using the NLSE.
Excepting the inertial contribution, values in the observed range are not shown in the upper right part of the figures, where small wavelength and high ice thickness is presented. Most of the values change at small wave numbers over the bandwidth of ice thickness and at small ice thickness over the bandwidth of wave number. Results of both, angular frequency and the velocity ratio, are similar, but for the velocity ratio the values of interest occur in a narrower range of ice thickness and wave number. This leads to the assumption that c_g/c_p is the critical constraint of Eqs. (24).
In detail, the sole bending contribution for the angular frequency, Subfig. (1.a), shows $\frac{d\omega}{dd} = 0$ for small wave numbers over the described characteristic area. In the reduced equationit becomes obvious that a small ice thickness and wave number yields the open water condition of angular frequency. The areas of open water condition are most present in the bending contribution, due to the proportionality of highly powered ice thickness and wave number ($\propto d^3, \propto k_0^5$).
In Subfig. (1.b) the velocity ratio is shown. In a similar characteristic range described for the angular frequency, the open water value $c_g/c_p = 0.5$ is reached. With equally increasing wave number and ice thickness the value increases.
The figures representing the sole inertia plot, Subfigs. (1.c) and (1.d) looks different. In the whole parameter space the values of both wave parameters are relevant and valid. The angular frequency for sole inertia contribution,

$$\omega_{0,I} = \left(\frac{gk_0}{1+Ik_0}\right)^{1/2} = \left(\frac{g}{1/k_0 + \rho_i d/\rho_w}\right)^{1/2}, \tag{25}$$

is characterized by the counteracting impact of wave number and ice thickness. If the inertia term vanishes (small d), again the open water solution is reached. But, due to the place in the denominator, the increasing inertia $I = (\rho_i d)/\rho_w$ causes a decrease of angular frequency at constant wave numbers with higher gradient for small waves and thicker ice. For fixed ice thickness the angular frequency increase due to the decreasing denominator caused by its vanishing 1/k term.
The velocity ratio reduces to

$$\frac{c_{g,I}}{c_{p,I}} = \frac{gk_0}{2(1+k_0I)^2(\omega_{0,I})^{3/2}}\,, \tag{26}$$

see Subfig. (1.d). In the upper right part of the figure the velocity range decrease to a level below the open water condition. This implies that inertia only marginally affect the deviation of the velocity ratio to the open water value. The superposition of sole flexural rigidity and inertia results in Subfigs. (2.a) and (2.b). The figures are highly correlated to the previously discussed sole bending figures. This redraws the dominant impact of the bending contribution due to the high power dependency on wave number and ice thickness. The inertia contribution only marginally varies the gradient of the velocity ratio within the characteristic range.
In Subfigs. (2.c) and (2.d) sole compression is represented. The values of angular frequency and velocity ratio is smaller in magnitude and validity range. The compression term is subtracted from the gravitational contributionFor increasing wave number and ice thickness both the frequency and the velocity ratio reaches zero. In contrast to previously discussed figures (bending and inertia contribution), where the values increase along the diagonal axis, the valid range is limited by a sharp zero-contour line.
Superposing all contribution, in fact, results in subtracting the compressive rigidity from the bending and inertia contribution. Subfigure (2.e) represents an area equal zero, respectively a non-valid range regarding Eq. (24). The inner limits of this area are defined by the compression, the outer limit is

Journal of Offshore Mechanics and Arctic Engineering. Received March 29, 2019;
Accepted manuscript posted November 19, 2019. doi:10.1115/1.4045625

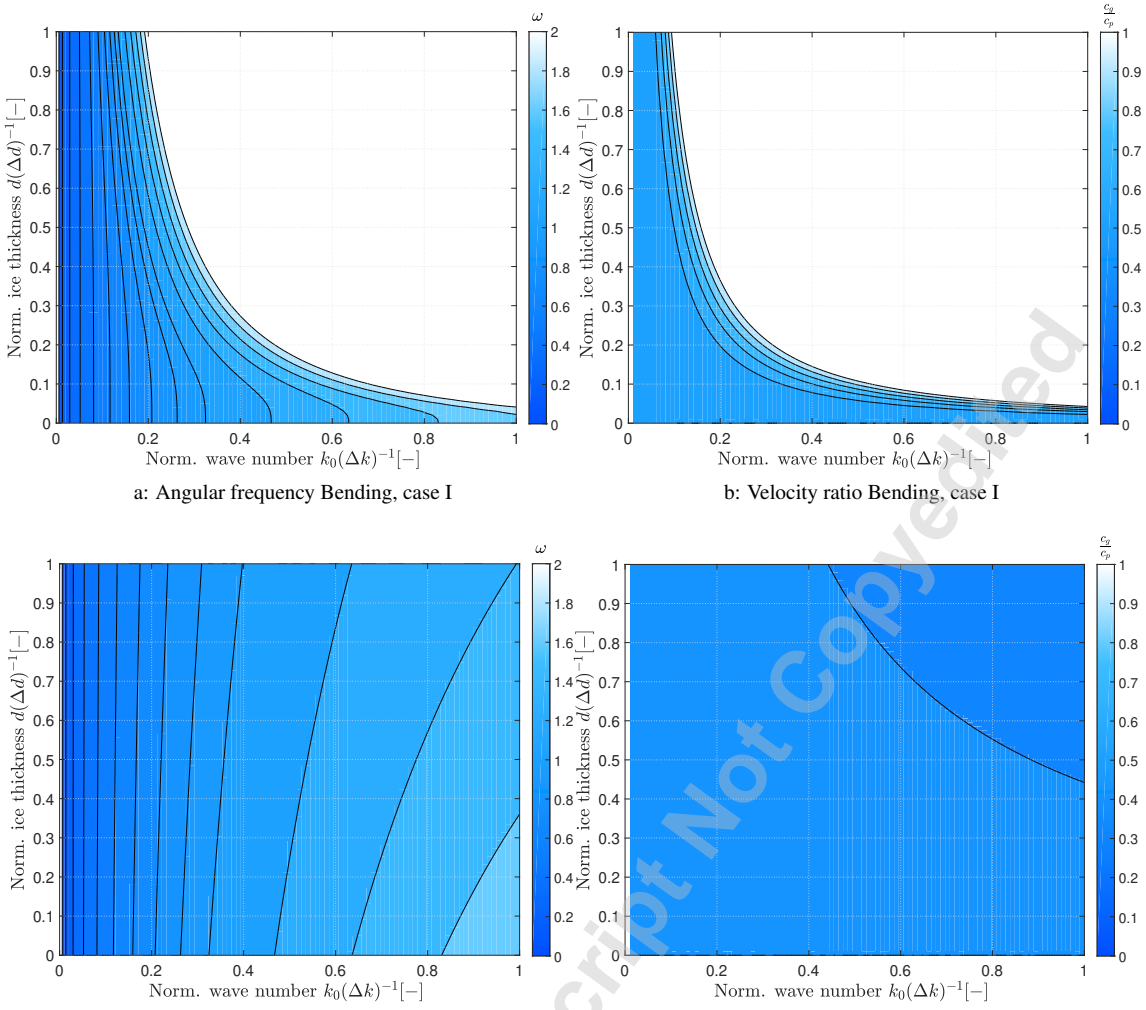

a: Angular frequency Bending, case I

b: Velocity ratio Bending, case I

c: Angular frequency Inertia, case II

d: Velocity ratio Inertia, case II

Fig. 1: Angular frequency (Subfigs. (a, c)) and ratio of group velocity to phase velocity (Subfigs. (b, d)) in parameter space of normalized wave number and ice thickness. Sole bending (Subfigs. (a, b)) and inertia contribution (Subfigs. (c, d)) to the wave parameters are shown. The angular frequency is limited to 0 to 2.0 the velocity ratio is in the range of 0 to 1.0. The range in which the wave number is varied, Δk, is given by $\{k_0 \in \mathbb{R} : 0\,\mathrm{m}^{-1} < k_0 \leq \pi/10\,\mathrm{m}^{-1}\}$. The ice thickness interval Δd is defined to $\{d \in \mathbb{R} : 0\,\mathrm{m} \leq d \leq 2\,\mathrm{m}\}$.

given by the inertia and bending contribution.
The corresponding result for the velocity range is more drastic. Nearly the complete sole compression properties are present and only a narrow, slightly-larger zero band at high ice thickness remains from the bending and inertia contribution.

Focusing ratio

As already mentioned a positive focusing ratio indicates the high likelihood of nonlinear focusing waves. Consequently the restriction

$$\frac{\beta}{\alpha} > 0 \tag{27}$$

has to be taken into account in addition to the constraints presented in Eq. (24) for the choice of the wave number and the ice thickness in the NLSE simulations.
In Figs. (3) and (4) the contributions of ice properties are shown in order of Tab. (1). As in the parameter study for angular frequency and velocity ratio shown, the relevant and valid values are in a similar figure area. The parameter analysis points out that the nonlinear wave-ice interaction based on the coefficients provided by Liu and Mollo-Christensen [11] is only valid in a narrow range of ice and wave properties. The limitations are given by the constraints Eqs. (24) and (27).
For simplicity, a schematic subdivision is introduced in Subfig. (3.d) using subquadrants, corresponding to wave and ice characteristics.
Subfigure (3.c) shows the superposition of sole bending and inertia contribution, Subfigs. (3.a) and (3.b). In subquadrant

Journal of Offshore Mechanics and Arctic Engineering. Received March 29, 2019;
Accepted manuscript posted November 19, 2019. doi:10.1115/1.4045625

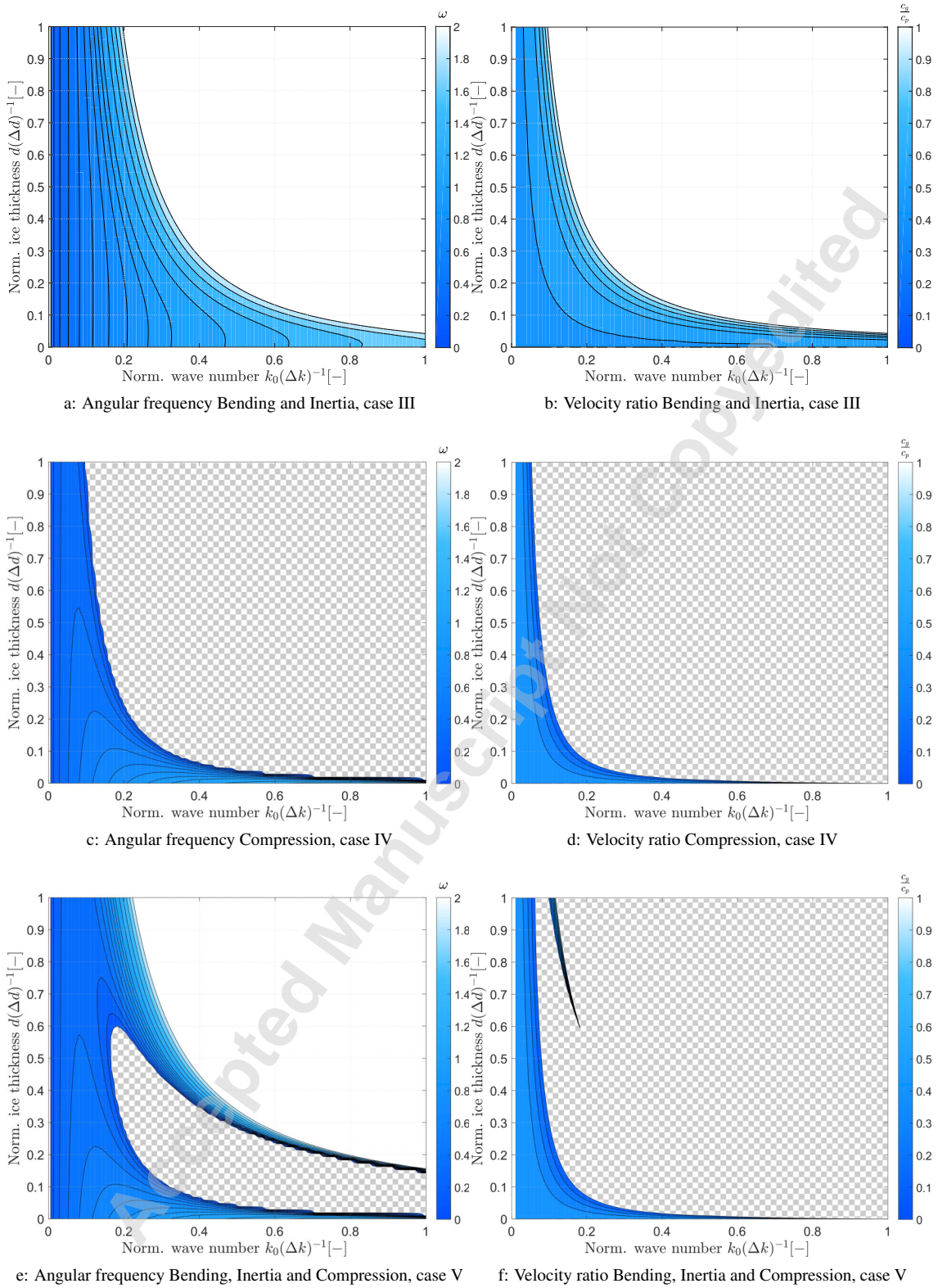

a: Angular frequency Bending and Inertia, case III

b: Velocity ratio Bending and Inertia, case III

c: Angular frequency Compression, case IV

d: Velocity ratio Compression, case IV

e: Angular frequency Bending, Inertia and Compression, case V

f: Velocity ratio Bending, Inertia and Compression, case V

Fig. 2: Angular frequency (Subfigs. (a, c, e)) and ratio of group velocity to phase velocity (Subfigs. (b, d, f)) in parameter space of normalized wave number and ice thickness for cases III-V. Shading represents non-valid areas regarding Eq. (24).

Journal of Offshore Mechanics and Arctic Engineering. Received March 29, 2019;
Accepted manuscript posted November 19, 2019. doi:10.1115/1.4045625

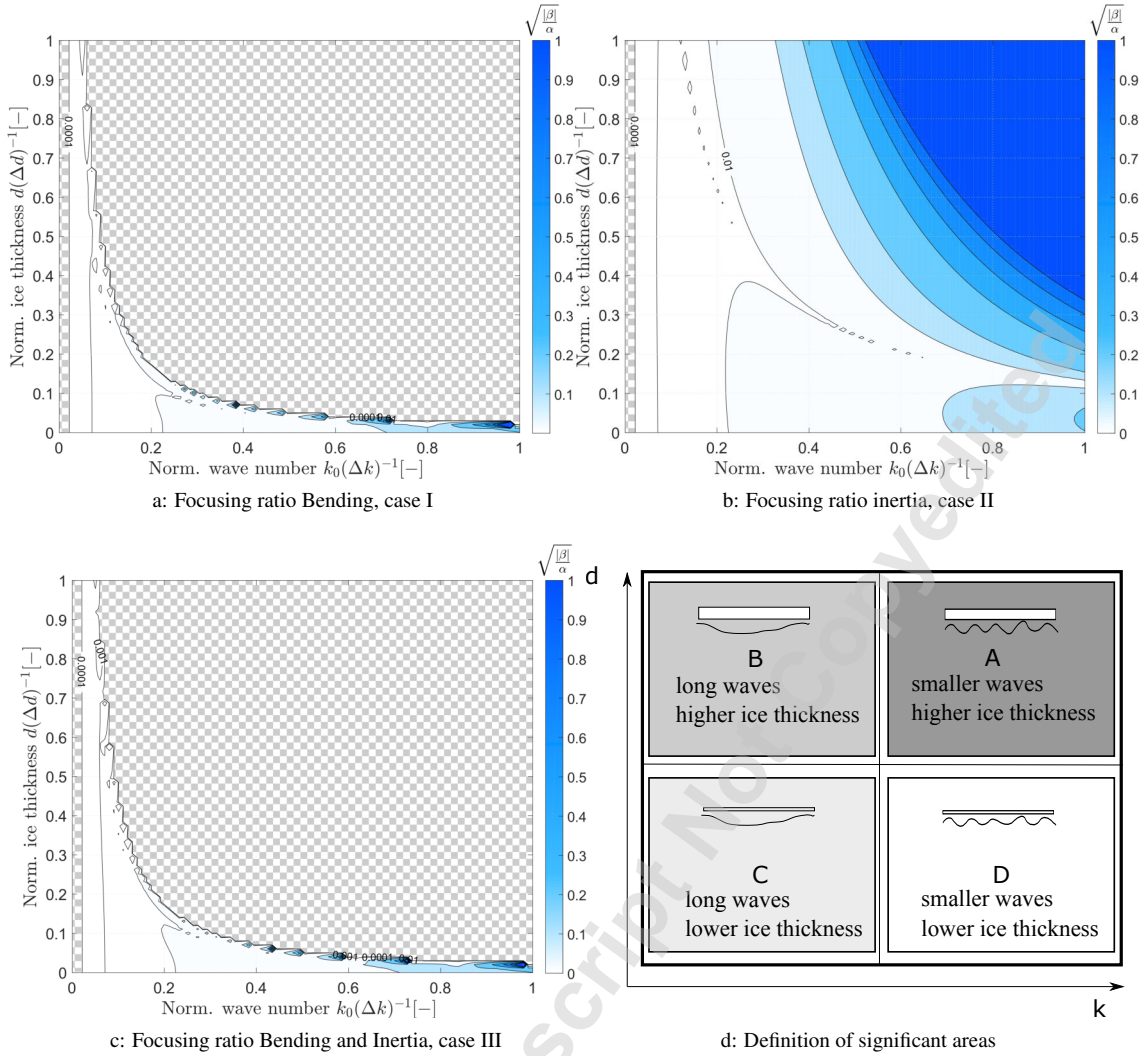

a: Focusing ratio Bending, case I

b: Focusing ratio inertia, case II

c: Focusing ratio Bending and Inertia, case III

d: Definition of significant areas

Fig. 3: Focusing ratio $\sqrt{\frac{|\beta|}{\alpha}}$ in parameter space of normalized ice thickness and wave number. In Subfig. (d) relevant subquadrants are defined regarding wave and ice characteristics. The ratio is shown in the range of 0 to 1.0. Shading represents non-valid areas regarding Eq. (27).

A the focusing ratio of the sole inertia contribution increases due to the higher ice thickness. In the case of the combined bending and inertia contribution and the sole bending contribution, spots of high focusing ratio lie on significant curves. The values are much larger than one. This implies that a fixed functional dependence on ice thickness and wave length trigger the instability of the nonlinear interactions. According to sole compression, Subfig. (4.a), the spots of high focusing ratios exist along two curves. Apart from this curves the focusing ratio increases in subquadrants A and D indepently from ice thickness.

In the superposition of bending, inertia and compression contribution, the three previously discussed significant curves are presented, see Subfig. (4.b). The high value areas are mostly spread in the range of small ice thickness and along the whole range of wave numbers, subquadrants C and D. The occurence of the focusing spots increase with increasing wave number and decreasing ice thickness. Reaching subquadrant B, again the curve of superposed bending and inertia contribution can be identified. In subquadrant A, at small waves and higher ice thickness, nonlinear focusing doesn't appear.

General comments on the parameter study

Compared to the sole concern of bending and compression, inertia only slightly impact the overall contribution. Reviewing Liu and Mollo-Christensen [11], it's found that the definitions for the compression proportion are given in terms of ice pack compression and the bending contribution is correlated to the ice plate properties. So both contributions are inherently defined in terms of larger dimensions. In contrast inertia, given by the, comparably small, water density ratio, scales only linearly with ice thickness. Physically an interpretation in terms of a two scale separation of the ice properties in the presence of wave dynamics seems obvious.

Journal of Offshore Mechanics and Arctic Engineering. Received March 29, 2019;
Accepted manuscript posted November 19, 2019. doi:10.1115/1.4045625

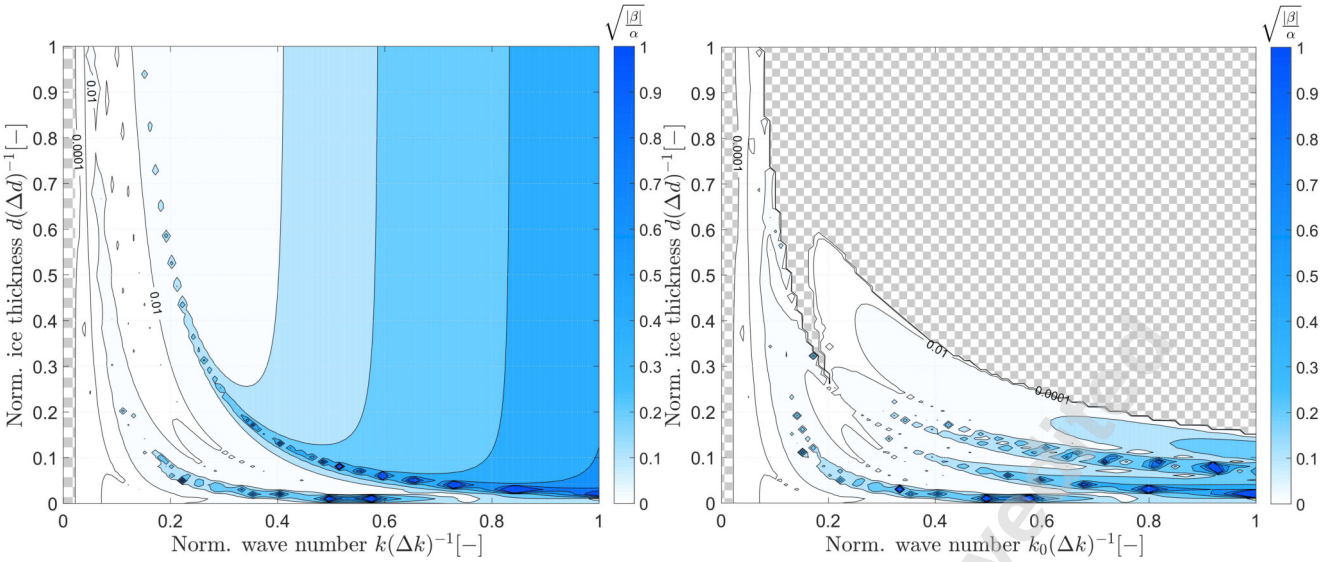

a: Focusing ratio Compression, case IV

b: Focusing ratio Bending, Inertia and Compression, case V

Fig. 4: Focusing ratio $\sqrt{\frac{|\beta|}{\alpha}}$ in parameter space of normalized ice thickness and wave number for sole compression and accounting all ice properties provided by Liu and Mollo-Christensen in [11]. The ratio is shown in the range of 0 to 1.0. The wave number bandwidth and the ice thickness are same as in Fig. 1.

Bending and compression are related to forces acting on large scales of the ice plate, whereas inertia is related to the hydrostatics of the ice, which can be reduced to the length scale of the submerged ice portion.

Furthermore, Liu and Mollo-Christensen concluded in their study that the pack ice compression is highly relevant for wave energy concentration. They argue that this is forced by both the mechanisms of very small group velocity and high nonlinear modulational instability due to the pack ice compression. The occurence of both small velocities and high focusing ratios (which are correlated to modulational instability, see Sec. 'Intense wave events') is also indicated by the results of the parameter study. Explicitly, the contours of significant large positive values in the focusing ratio (Fig. (4b)) and the contours of small velocity ratios (Fig. (2f)) occur in the same area in the parameter range.

The dominant role of compression is also represented in the results. Comparing the figures of all ice material properties (Figs. (2e), (2f) , (4b)) with the sole contribution of compression (Figs. (2c), (2d), (4a)) and the contribution of combined bending and inertia (Figs. (2a), (2b) , (3c)), the dominance of compression to ice properties is evident.

The sign reversals of nonlinear and dispersive terms in the NLSE (negative focusing ratio), also observed by Liu and Mollo-Christensen, correspond to the introduced limitations (Eqs. (24) and (27)). In our study we pointed out that the sign reversals in the focusing ratio are correlated to the non physical negative wave number and velocity ranges. This is shown by the similarity of 'non-valid' (chessboard marked) regimes in the velocity ratio, the angular frequency and the focusing ratio.

Advanced approaches

Alternatively, the elastic deformation of the ice plate could be formulated in terms of the dynamic equation of motion with forcing by the nonlinear dynamic boundary condition of the waves. The terms of inertia, damping and stiffness could be defined by the small scale material properties of flexural and compressive rigidity and inertia. The damping of the ice plate could be derived from the inertia and stiffness of the plate and eigenfrequencies could be analyzed regarding wave's angular frequencies. Furthermore the attenuation of the wave due to viscous effects resulting from wave-ice interaction has to be quantified and accounted in terms of introducing a corresponding coefficient, see for example Marchenko et al. [36] and Guyenne et al. [37].

The nonlinear boundary conditions for the waves may be reviewed in terms of identifying the ice plates bottom with wave's surface elevation. This holds, if the ice plate is assumed to be thin. For larger length scales, the dependence of wave kinematic's on the water depth is significant. Thus the bottom of the mainly submerged ice plate is not necessarily exposed to the surface condition of the wave, but to smaller orbital motions below the water surface.

NLSE time domain simulation with open water and ice boundary condition

For some specific nonlinear wave events the NLSE has analytic solutions. These events are divided in categories of nonlinear wave groups, two of this are the breather and the envelope solitons. The Peregrine breather is one breather solution, which was initially derived by Peregrine [38] and is given in terms of the linear and nonlinear NLSE coefficients

Journal of Offshore Mechanics and Arctic Engineering. Received March 29, 2019;
Accepted manuscript posted November 19, 2019. doi:10.1115/1.4045625

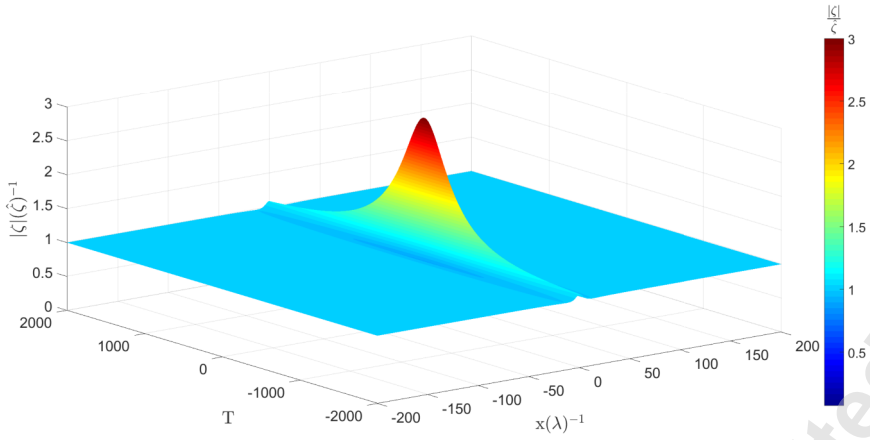

a: Open, deep water

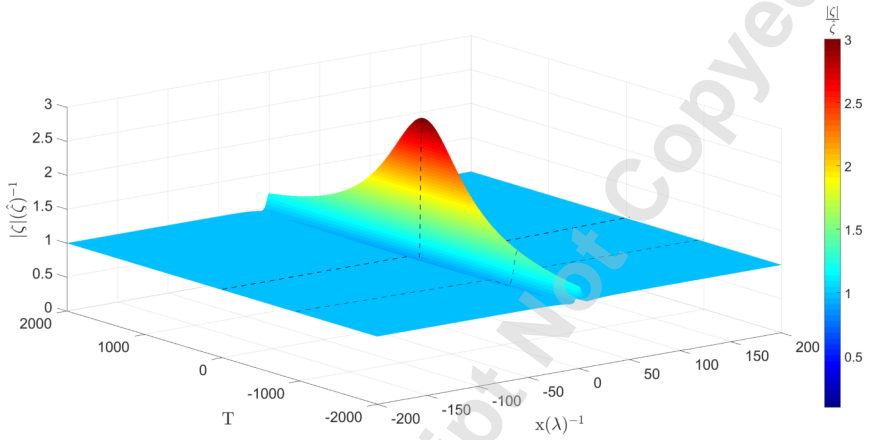

b: Ice covered, deep water

Fig. 5: Analytic solution of Peregrine Breather in open, Subfig. (a), and ice covered water, Subfig. (b), for normalized x-t parameter space $\{x(\lambda)^{-1} \in \mathbb{R} : -2.0\times10^2\,\mathrm{m}(\lambda)^{-1} \le x(\lambda)^{-1} \le 2.0\times10^2\,\mathrm{m}(\lambda)^{-1}\}$ and $\{T \in \mathbb{R} : -2.0\times10^3 \le T \le 2.0\times10^3\}$. Light and dark dotted lines in Subfig (b) marks location of t_{start} and t_{target}.

by [39]

$$A(x,t) = A_0 \exp\left(-i\beta A_0^2 t\right)\cdot \cdot\left(\frac{4(1-i2\beta A_0^2 t)}{1+4\beta^2 A_0^4 t^2 + 2\beta/\alpha A_0^2 (x-c_g t)^2} - 1\right). \quad (28)$$

In open water wave tank experiments, e.g. Chabchoub et al. [40], the occurence of the Peregrine breather could shown experimentally.

In this section the Peregrine breather, see Eq. (28), is discussed by the comparison of the open, deep water condition, see alpha and beta Eq. (10), and the ice-covered, deep water condition given by Liu and Mollo-Christensen [11], see Eq. (19). As initial condition of the NLSE the surface elevation at initial time (space series) is necessary, which is calculated by the analytic equation of the Peregrine breather. Direct numerical simulations are performed and the results are compared to the exact solutions in order to verify the numerical procedure.

Peregrine breather in open water

The space series of the open, deep water cenvelope is presented in Subfig. ((6).a) for two discrete time steps. The NLSE simulation coincide with the analytic Peregrine solutions. The elevation and envelopes represents the characteristic and excepted shape of the Peregrine breather.

Peregrine breather in ice covered water

In this section the space series of the Peregrine breather and the corresponding NLSE simulations in ice covered water are shown in Subfig ((6).b).

For the simulation, the values for Young's modulus, the densities and the Poisson ratio were taken from Liu and Mollo-Christensen [11]. Note that compression is suppressed in this simulation setup, which results in different wave number and ice thickness compared to the ones provided by Liu and Mollo-Christensen [11]. To find the corresponding values, we use Fig. (3.c), choose $k_0/\Delta k = 0.586$ and find the correlated ice thickness to be $d/\Delta d = 0.0303$. The wave group envelopes of the analytical solution and the direct simulations

Journal of Offshore Mechanics and Arctic Engineering. Received March 29, 2019;
Accepted manuscript posted November 19, 2019. doi:10.1115/1.4045625

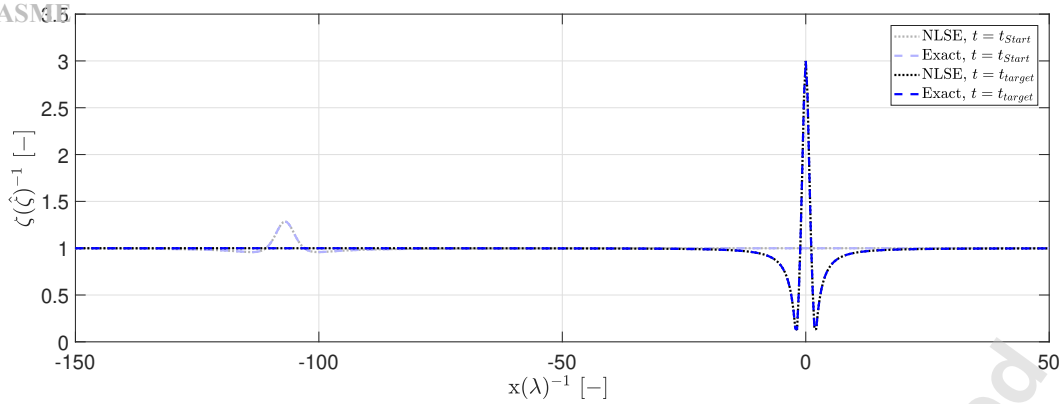

a: Open water solutions for $|\zeta|$ in interval $\{x(\lambda)^{-1} \in \mathbb{R} : 1.0 \times 10^4\,\mathrm{m}(\lambda)^{-1} \leq x(\lambda)^{-1} \leq 2.0 \times 10^4\,\mathrm{m}(\lambda)^{-1}\}$

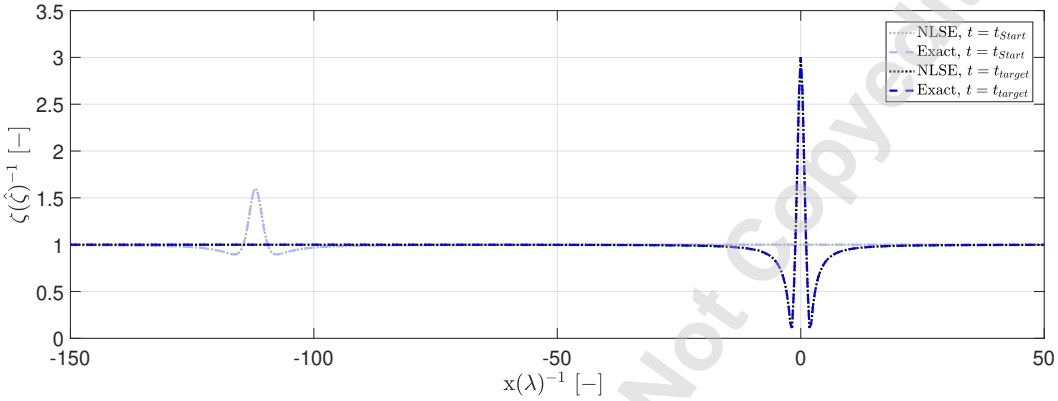

b: Ice covered water solution for $|\zeta|$ in interval $\{x(\lambda)^{-1} \in \mathbb{R} : 1.0 \times 10^4\,\mathrm{m}(\lambda)^{-1} \leq x(\lambda)^{-1} \leq 2.0 \times 10^4\,\mathrm{m}(\lambda)^{-1}\}$

Fig. 6: Comparison of open water, Subfig. (a), and ice covered, Subfig. (b),), deep water condition NLSE simulation and exact solution of Peregrine breather by means of, with respect to wavelength, normalized envelope of the wave group at wave number $k_0 = 0.1841\,\mathrm{m}^{-1}$, wave steepness $\varepsilon = 0.05$ and ice thickness $d = 0.061\,\mathrm{m}$. The properties for ice are defined with the flexural rigidity and the length scale of submerged ice portion, the **compressive strength is equal to zero**. The timestep of simulation is $dt = 0.1\,\mathrm{s}$. The blue, dashed lines represent exact solution, black dotted lines gives elevation of NLSE simulations.

coincide (6.b)) verify the implemented numerical procedure based on the split-step method. Although the surface condition in the ice-case differs strongly from the open water condition, the Peregrine breather characteristics are comparable.

In Fig. (5) both the open and ice covered solution for the analytic Peregrine solution are represented. Under the same normalized temporal and spatial domain it's figured out that the ice covered solution is located in a narrower space and time range.

Conclusion

In the first part of the paper, relevant aspects of wave theory and ice material theory are reviewed and the present work is put into the theoretical framework. The ice boundary condition given by Liu and Mollo-Christensen [11] is introduced and discussed in the context of the space nonlinear Schrödinger equation.

A parametric study is used to analyze the effect of flexural rigidity, compressive stress, and ice thickness to the wave dispersion, ratio of group to phase velocity, and the ratio of the two NLSE coefficients. By looking at the properties independently and in combination, the influence of each parameter is figured out.

First, the parameters are limited to physical consistency, which entails only positive parameters. The range of the parameters is limited to order of one. Under this constraints, the range of ice thickness and wave numbers leading to valid specifications decrease. Mostly, small waves and high ice thickness leads to values which are either not valid in terms of the constraints or larger than order of one.

In terms of the wave specifications, the velocity ratio shows narrower areas of valid values in the investigated parameter space and is thus assumed to be the more critical parameter compared to the angular frequency.

In terms of the focusing ratio, the superposition of all contributions results in a figure where significant curves of high focusing ratios occur. These curves represent the valid and relevant curvature for nonlinear focusing waves. The corresponding ice thickness and wave number give the control parameters for the NLSE simulation setup.

By comparing the sole contributions with respect to the three observed parameters angular frequency, velocity ratio and focusing ratio, it is visualized that inertia's impact is small compared to the contributions of bending and compression. This can be explained by the scale separation, which is provided by the ice properties' definition in Liu and Mollo-Christensen [11]. For the focusing ratio one can claim additionally that by the interaction of bending and compression the nonlinear instability diminishes locally in areas of smaller wave length.

Furthermore, the deviation from the open water values are analyzed. The different functional relations of the wave parameters, with respect to ice thickness and wave number, indicate that the deviations to the open water solutions increase at certain combinations of wave number and ice thickness. This certain combinations represent the critical ice thickness and wave length at which the ice plate influence the wave dynamics.

In the second part of the presented results, the Peregrine breather is simulated with the NLSE under open water and ice covered water condition. The validation of the results is done by comparing the existing analytical solution and the NLSE simulations. For assuming both open and ice boundary condition the space series coincide with each other. The Peregrine breather characteristic can be reproduced under the presence of ice. Comparison between direct numerical simulations and the exact solution verified the numerical approach. Thus, this numerical procedure can be used for systematic numerical investigations on different wave system where exact solutions are not available. The control parameters for the ice covered simulation, wave number and ice thickness, are chosen with the figures from the parameter study, so that the defined constraints are fulfilled. The occurence of the analytic surface elevation and envelope of the Peregrine breather verifies the choice of the control parameters for likely nonlinear focusing. By this, the results of the parameter study are exemplarily illustrated.

Finally, the analytic solutions of the open and ice bounded Peregrine breather are shown in the space-time domain. The increase in time for the evolution of the breather solution due to the ice cover is demonstrated.

For subsequent research, the material properties and their definitions, provided in Liu and Mollo-Christensen [11], have to be reviewed. Especially the attenuation of the waves have to be represented by a refined model. The relevance of compression in the absence of large scale ridge formation has to be evaluated. Smaller scale processes and their impact on the overall material behavior have to be taken into account. Furthermore a systematic investigations with realistic sea states has to be applied.

Acknowledgements

This paper is published as a contribution to the research project "Nonlinear wave-ice-interaction" KL 3246/1-1. The authors wish to express their gratitude to the German Research Foundation *DFG* for funding and supporting this research project.

References

[1] Harvey, B. J., Shaffrey, L. C., and Woollings, T. J., 2015. "Deconstructing the climate change response of the northern hemisphere wintertime storm tracks". *Climate dynamics,* **45**(9-10), pp. 2847–2860.

[2] Wuebbles, D., Fahey, D., Hibbard, K., Dokken, D., Stewart, B., and Maycock, T., 2017. Climate science special report: Fourth national climate assessment, volume i. Tech. rep., U.S. Global Change Research Program.

[3] Masson-Delmotte, V., Zhai, P., Pörtner, H., Roberts, D., Skea, J., Shukla, P., Pirani, A., Moufouma-Okia, W., Péan, C., Pidcock, R., Connors, S., Matthews, J. B. R., Chen, Y., Zhou, X., Gomis, M. I., Lonnoy, E., Maycock, T., Tignor, M., and Waterfield, T. e., 2018. "IPCC, 2018: Summary for policymakers". *IPCC Special Report*.

[4] Li, J., Ma, Y., Liu, Q., Zhang, W., and Guan, C., 2019. "Growth of wave height with retreating ice cover in the arctic". *Cold Regions Science and Technology,* **164**, p. 102790.

[5] Morim, J., Hemer, M., Wang, X. L., Cartwright, N., Trenham, C., Semedo, A., Young, I., Bricheno, L., Camus, P., Casas-Prat, M., Erikson, L., Mentaschi, L., Mori, N., Shimura, T., Timmermans, B., Aarnes, O., Breivik, O., Behrens, A., Dobrynin, M., Menendez, M., Staneva, J., Wehner, M., Wolf, J., Kamranzad, B., Webb, A., Stopa, J., and Andutta, F., 2019. "Robustness and uncertainties in global multivariate wind-wave climate projections". *Nature Climate Change*, pp. 1–8.

[6] Stephenson, S. R., Smith, L. C., and Agnew, J. A., 2011. "Divergent long-term trajectories of human access to the arctic". *Nature Climate Change,* **1**(3), pp. 156–160.

[7] Liu, M., and Kronbak, J., 2010. "The potential economic viability of using the northern sea route (nsr) as an alternative route between asia and europe". *Journal of Transport Geography,* **18**(3), pp. 434–444.

[8] Von Bock und Polach, R. U. F., Ehlers, S., and Erikstad, S., 2015. "A decision-based design approach for ships operating in open water and ice". *Journal of Ship Production and Design,* **31**(4).

[9] Whitham, G., 1967. "Non-linear dispersion of water waves". *Journal of Fluid Mechanics,* **27**(2), pp. 399–412.

[10] Osborne, A. R., Onorato, M., and Serio, M., 2000. "The nonlinear dynamics of rogue waves and holes in deep-water gravity wave trains". *Physics Letters A,* **275**(5-6), pp. 386–393.

[11] Liu, A., and Mollo-Christensen, E., 1988. "Wave propagation in a solid ice pack". *Journal of Physical Oceanography*.

[12] Collins, C., Rogers, E., Marchenko, A., and Babanin, A., 2015. "In situ measurement of an energetic wave event in the arctic marginal ice zone". *Geophysical Research Letters,* **42**, pp. 1863–1870.

[13] Kohout, A., Williams, M., Dean, S., and Meylan, M., 2014. "Storm induced sea ice breakup and the implica-

tions for ice extent". *Nature,* **509**, pp. 604–617.

[14] Lamb, H., 1932. *Hydrodynamics*. Cambridge university press.

[15] Bronstein, I. N., Semendjajew, K. A., Musiol, G., and Mühlig, H., 2013. *Taschenbuch der Mathematik*, 9 ed., Vol. 1. Springer-Verlag.

[16] Whitham, G., 2011. *Linear and Nonlinear Waves*, Vol. 42. John Wiley & Sons.

[17] Kundu, P. K., Cohen, I. M., and Dowling, D. W., 2016. *Fluid Mechanics*, 6th ed. Academic Press.

[18] Bracewell, R., 2000. *The Fourier Transform and Its Applications*. Electrical engineering series. McGraw Hill.

[19] Gerstner, F., 1802. Theorie der wellen: Abhandlungen der koniglichen bohmischen gesellschaft der wissenschaften.

[20] Stokes, G. G., 1847. "On the theory of oscillatory waves". *Camb. Trans.,* **8**, p. 441.

[21] Zakharov, V., 1968. "Stability of periodic waves of finite amplitude on the surface of a deep fluid". *Zhurnal Prikladnoi Mekhaniki i Tekhnicheskoi Fiziki*.

[22] Davey, A., and Stewartson, K., 1974. "On three-dimensional packets of surface waves". *Proceedings Royal Society London,* **338**(1613), pp. 101–110.

[23] Holmes, M. H., 2012. *Introduction to perturbation methods*, Vol. 20. Springer Science & Business Media.

[24] Onorato, M., Residori, S., Bortolozzo, U., Montina, A., and Arecchi, F., 2013. "Rogue waves and their generating mechanism in different physical contexts". *Physics Reports*.

[25] Serio, M., Onorato, M., Osborne, A. R., and Janssen, P., 2005. "On the computation of the benjamin-feir index". *Il nuovo cimento della Società Italiana di Fisica,* **2**, p. 0.

[26] Weideman, J., and Herbst, B., 1986. "Split-step methods for the solution of the nonlinear schrödinger equation". *SIAM Journal on Numerical Analysis,* **23**(3), pp. 485–507.

[27] Tappert, F., 1974. "Numerical solutions of the korteweg-de vries equation and its generalizations by the split-step fourier method". *Nonlinear Wave Motion,* **15**, pp. 215–216.

[28] Kharif, C., Pelinovsky, E., and Slunyaev, A., 2009. *Rogue Waves in the ocean*. Springer Verlag.

[29] Benjamin, T., and Feir, J., 1967. "The disintegration of wave trains on deep water". *Journal of Fluid Mechanics,* **27**(3), pp. 417–430.

[30] Benney, D., 1962. "Non-linear gravity wave interaction". *Journal of Fluid Mechanics,* **14**(4), pp. 577–584.

[31] Timco, G. W., and Weeks, W. F., 2010. "A review of the engineering properties of sea ice". *Cold Regions Science and Technology,* **60**(2), pp. 107–129.

[32] Frankenstein, G., and Garner, R., 1967. "Equations for determining the brine volume of sea ice from -0.5° to -22.9°c.". *Journal of Glaciology,* **6**(48), p. 943–944.

[33] Timco, G. W., and O.'Brien, S., 1994. "Flexural strength equation for sea ice". *Cold Regions Science and Technology,* **22**(3), pp. 285–298.

[34] Riska, K., Wilhelmson, M., Englund, K., and Leiviskä, T., 1998. Performance of merchant vessels in ice in the baltic. Tech. rep., Finnish Maritime Administration, December.

[35] Kevrekidis, P. G., Frantzeskakis, D. J., and Carretero-González, R., 2015. *The defocusing nonlinear Schrödinger equation: from dark solitons to vortices and vortex rings*. SIAM.

[36] Marchenko, A., 2016. "Damping of surface waves propagating below solid ice". In The 26th International Ocean and Polar Engineering Conference, International Society of Offshore and Polar Engineers.

[37] Guyenne, P., and Parau, E. I., 2017. "Numerical simulation of solitary-wave scattering and damping in fragmented sea ice". In The 27th International Ocean and Polar Engineering Conference, International Society of Offshore and Polar Engineers.

[38] Peregrine, D., 1983. "Water waves, nonlinear schrödinger equations and their solutions". *The ANZIAM Journal,* **25**(1), pp. 16–43.

[39] Klein, M., 2015. "Tailoring critical wave sequences for response based design". PhD thesis, Technische Universität Berlin.

[40] Chabchoub, A., Hoffmann, N., and Akhmediev, N., 2011. "Rogue wave observation in a water wave tank". *Physical Review Letters,* **106**(20), p. 204502.

List of Figures

1 Angular frequency (Subfigs. (a, c)) and ratio of group velocity to phase velocity (Subfigs. (b, d)) in parameter space of normalized wave number and ice thickness. Sole bending (Subfigs. (a, b)) and inertia contribution (Subfigs. (c, d)) to the wave parameters are shown. The angular frequency is limited to 0 to 2.0 the velocity ratio is in the range of 0 to 1.0. The range in which the wave number is varied, Δk, is given by $\{k_0 \in \mathbb{R} : 0\,\mathrm{m}^{-1} < k_0 \leq \pi/10\,\mathrm{m}^{-1}\}$. The ice thickness interval Δd is defined to $\{d \in \mathbb{R} : 0\,\mathrm{m} \leq d \leq 2\,\mathrm{m}\}$. . . 7

2 Angular frequency (Subfigs. (a, c, e)) and ratio of group velocity to phase velocity (Subfigs. (b, d, f)) in parameter space of normalized wave number and ice thickness for cases III-V. Shading represents non-valid areas regarding Eq. (24). 8

3 Focusing ratio $\sqrt{\frac{|\beta|}{\alpha}}$ in parameter space of normalized ice thickness and wave number. In Subfig. (d) relevant subquadrants are defined regarding wave and ice characteristics. The ratio is shown in the range of 0 to 1.0. Shading represents non-valid areas regarding Eq. (27). 9

4 Focusing ratio $\sqrt{\frac{|\beta|}{\alpha}}$ in parameter space of normalized ice thickness and wave number for sole compression and accounting all ice properties provided by Liu and Mollo-Christensen in [11]. The ratio is shown in the range of 0 to 1.0. The wave number bandwidth and the ice thickness are same as in Fig. 1. 10

5 Analytic solution of Peregrine Breather in open, Subfig. (a), and ice covered water, Subfig. (b), for normalized x-t parameter space $\{x(\lambda)^{-1} \in \mathbb{R} : -2.0 \times 10^2\,\mathrm{m}(\lambda)^{-1} \leq x(\lambda)^{-1} \leq 2.0 \times 10^2\,\mathrm{m}(\lambda)^{-1}\}$ and $\{T \in \mathbb{R} : -2.0 \times 10^3 \leq T \leq 2.0 \times 10^3\}$. Light and dark dotted lines in Subfig (b) marks location of t_{start} and t_{target}. 11

6 Comparison of open water, Subfig. (a), and ice covered, Subfig. (b),), deep water condition NLSE simulation and exact solution of Peregrine breather by means of, with respect to wavelength, normalized envelope of the wave group at wave number $k_0 = 0.1841\,\mathrm{m}^{-1}$, wave steepness $\varepsilon = 0.05$ and ice thickness $d = 0.061\,\mathrm{m}$. The properties for ice are defined with the flexural rigidity and the length scale of submerged ice portion, the **compressive strength is equal to zero**. The timestep of simulation is $dt = 0.1\,\mathrm{s}$. The blue, dashed lines represent exact solution, black dotted lines gives elevation of NLSE simulations. 12

List of Tables

1 Variation of assumed ice properties, **B**ending, **C**ompression and **I**nertia and corresponding figures. For '1' the appropriate term is taken into account, for '0' the term is set to zero. 6